

## Research article

# The Effect of PbS Colloidal Quantum Dots with CdS and ZnS Coating on Photovoltaic Properties

Napasuda Wichaiyo<sup>1\*</sup>, Mettaya Kitiwan<sup>1,2</sup>, Qing Shen<sup>3</sup> and Witoon Yindeesuk<sup>1,2</sup>

<sup>1</sup>Department of Physics, School of Science, King Mongkut's Institute of Technology Ladkrabang, Bangkok, Thailand

<sup>2</sup>Devices and Systems for Energy and Environment Research Unit, School of Science, King Mongkut's Institute of Technology Ladkrabang, Bangkok, Thailand

<sup>3</sup>Department of Engineering Science, Graduate School of Informatics and Engineering, The University of Electro-communications, Tokyo, Japan

Received: 23 May 2022, Revised: 7 July 2022, Accepted: 6 September 2022

DOI: 10.55003/cast.2022.02.23.011

### Abstract

#### Keywords

co-precipitation method;  
dip-coating method;  
lead(ii) sulfide colloidal quantum dots;  
photovoltaic cells;  
successive ionic layer adsorption and reaction method

In this research, we used the co-precipitation method to fabricate lead sulfide colloidal quantum dots (PbS CQDs) for photovoltaic cells. PbS CQDs were deposited uniformly on a titanium dioxide electrode by the dip-coating method. Photoelectrodes were prepared by coating layers using the successive ionic layer adsorption and reaction (SILAR) method. A solar simulation was used to investigate the photovoltaic properties of photoelectrodes under one sun illumination (100 mW/cm<sup>2</sup>) at room temperature (AM 1.5 G). The photovoltaic measurements demonstrated that TiO<sub>2</sub>/PbS CQDs with CdS and ZnS coating electrodes had a maximum power conversion efficiency (PCE) of 1.01 %. The crystallite size of PbS CQDs with different coating layers was analyzed using X-ray diffraction (XRD), and the crystallite size range was 6-7 nm. The existence of PbS CQDs and coating layers on the TiO<sub>2</sub> electrodes was confirmed by scanning electron microscopy (SEM) and energy dispersive X-ray spectroscopy (EDS). UV-visible spectroscopy was used to obtain the optical properties of the photoelectrodes. The optical band gap was 0.72-0.75 eV.

## 1. Introduction

Quantum dots are nanoparticles, and are considered a fascinating alternative for use in inorganic semiconductors such as laser, infrared detectors, and photovoltaic cells. Colloidal quantum dots (CQDs) are nanostructures covered by surfactant molecules or ligands and dispersed in a solution. Their electrical and optical properties are unique, with the optical band gap and absorption spectra

\*Corresponding author: E-mail: 63605027@kmitl.ac.th

corresponding to particle size and multiple exciton generation (MEG), making them intriguing fabrication alternatives [1-4]. CQDs are commonly synthesized using the hot injection method, which requires rapidly injecting an organometallic precursor into a high boiling point solvent ( $>150^{\circ}\text{C}$ ) under a nitrogen atmosphere. The hot injection method separates the nucleation and growth phases, resulting in high-quality quantum dots with a controlled size distribution [5-8]. The high temperatures under  $\text{N}_2$  flow are one of the disadvantages of the hot injection method. It is too difficult for beginners and cannot be easily prepared in a typical ambience.

Rosiles-Perez *et al.* [1] studied the precipitation procedure between cationic and anionic solutions under ultrasonic irradiation to form the required PbS CQDs. PbS CQDs are particularly impressive semiconductor materials since the optical band gap of PbS perfectly matches the infrared spectra wavelength range, which means they can efficiently absorb photon energy for photovoltaic cell light-harvesting [9]. PbS CQDs have sometimes been synthesized using ultrasound-assisted precipitation instead of the hot injection method. Unfortunately, this involves an absence of ligands that can form protective surface layers. The nanoparticles tend to form agglomerates and lose their monodispersed colloidal particle structure, including long-term colloidal stability. In contrast, the co-precipitation method is an uncomplicated procedure applied to synthesize inorganic compounds. It is the precipitation of a typically soluble component involving the creation of mixed crystals, adsorption, and mechanical entrapment [10]. In this research, we modified the synthesis of PbS CQDs by using co-precipitation instead of ultrasound-assisted precipitation. The photovoltaic properties were studied for enhancement by changing coating conditions with CdS and ZnS layers [11, 12].

## 2. Materials and Methods

A photovoltaic cell is composed of three main components: the photoelectrode (or working-electrode), the electrolyte, and the counter electrode. The structures of a photovoltaic cell and a counter electrode are shown in Figure 1, and the preparation information is provided below.

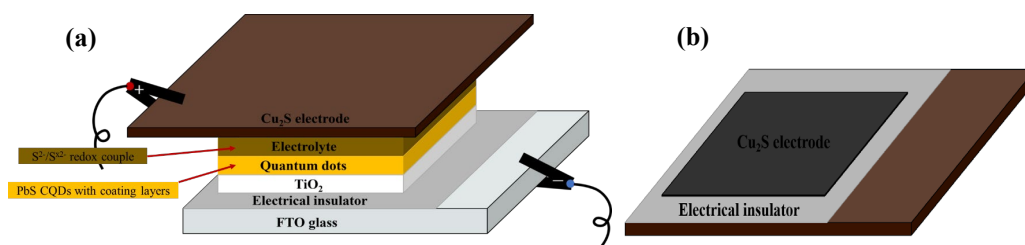


**Figure 1.** Schematic diagram structures of (a) a photovoltaic cell and (b) a counter electrode

### 2.1 Materials

For the preparation of the photovoltaic cell: lead(II) nitrate ( $\text{Pb}(\text{NO}_3)_2$ ), sodium sulfide ( $\text{Na}_2\text{S}\cdot 9\text{H}_2\text{O}$ ), cadmium nitrate ( $\text{Cd}(\text{NO}_3)_2\cdot 4\text{H}_2\text{O}$ ), zinc acetate ( $\text{Zn}(\text{CH}_3\text{COO})_2\cdot 2\text{H}_2\text{O}$ ), oleic acid ( $\text{C}_{18}\text{H}_{34}\text{O}_2$ ), chloroform ( $\text{CHCl}_3$ ), hydrochloric acid ( $\text{HCl}$ ), sulfur ( $\text{S}$ ) and titanium dioxide ( $\text{TiO}_2$ ) were purchased from Sigma-Aldrich.

## 2.2 Preparation of the photoelectrode

A titanium dioxide (TiO<sub>2</sub>) layer was coated using the doctor blading method on a fluorine-doped tin oxide (FTO) substrate of area 4 cm<sup>2</sup>, followed by drying at room temperature for 15 min and sintered at 500°C for 30 min. The TiO<sub>2</sub> layer on FTO glass had a thickness of 5 μm, and the active area of all photoelectrodes was 0.25 cm<sup>2</sup>. In addition, three devices were measured for each condition to obtain the properties of photovoltaic cells.

PbS CQDs were synthesized using the co-precipitation method. 0.02 M of lead nitrate was gradually added to 0.02 M of sodium sulfide in a beaker. Subsequently, we obtained PbS solids in solution, which were then annealed them at 95°C for 3 h. The PbS solids were added to a beaker in an oil bath at 160-170°C for 5 min. After that, 10.3 mmol of oleic acid was added and mixed for 10 min. The beaker in the oil bath was then put in an ice bath for 5 min before being transferred onto a magnetic stirrer and stirred at room temperature for 15 min. The particle size was selected by centrifugation at 3,000 rpm and 5,000 rpm for 5 min and 10 min, respectively, and the precipitate was removed from the tube. 10 mL of chloroform solution was then added to the tube. Then, the PbS CQDs dispersed in chloroform solution were obtained. Each TiO<sub>2</sub> electrode was immersed into the PbS CQDs solution twice for 1 min per time using the dip-coating method.

CdS and ZnS layers were prepared by the SILAR method. Cd(NO<sub>3</sub>)<sub>2</sub> at a concentration of 0.05 M was used as the cationic solution, and Na<sub>2</sub>S solution at a concentration of 0.05 M was used as anionic solution for forming CdS layers. Zn(CH<sub>3</sub>COO)<sub>2</sub> at concentration of 0.1 M was used as the cationic solution, and Na<sub>2</sub>S solution with a concentration of 0.1 M was used as anionic solution for forming ZnS layers. The TiO<sub>2</sub>/PbS CQD electrode was immersed in the cation solution for 1 min, then washed with methanol. After that, it was immersed in the anion solution for 1 min, then washed with methanol. This technique was performed five times for the CdS layers and two times for the ZnS layers.

## 2.3 Preparation of the electrolyte

The photoelectrode was separated by a redox electrolyte or hole conductor from the counter electrode. The electrolyte was made by mixing 10 ml of DI water, 0.34 g of sulfur, and 2.44 g of Na<sub>2</sub>S at 45°C for 2 h.

## 2.4 Preparation of the counter electrode

The counter electrode was prepared by immersing a copper sheet of area 4 cm<sup>2</sup> in HCl solution at 70-75°C for 5 min. An electrical insulator was used to restrict the active area to 0.25 cm<sup>2</sup>. The polysulfide electrolyte was then dropped onto the active area of the copper surface. As a result, the Cu<sub>2</sub>S counter electrode was created.

## 2.5 Characterizations

FEI, Quanta 250 scanning electron microscopy (SEM), and energy-dispersive X-ray spectroscopy (EDS) were used to study the photoelectrode characteristics and the existence of CdS and ZnS on TiO<sub>2</sub>/PbS CQDs electrode's surface. The crystal structure and crystallite size were analyzed using Rigaku, MiniFlex X-ray diffraction (XRD). UV-visible spectroscopy (Shimadzu, UV-2600i) was used to obtain the optical properties. The photovoltaic properties of the TiO<sub>2</sub>/PbS CQDs electrodes with coating layers were investigated using a Keithley 2400 with 150 W short-arc Xe lamp light source solar simulation (Peccell Technologies, PEC-L11) at room temperature under one sun (100 mW/cm<sup>2</sup>) and higher (A.M. 1.5G, Effective illumination area).

### 3. Results and Discussion

PbS QDs with various coating layers were deposited on the  $\text{TiO}_2$  surface, as illustrated in Figure 2. The thickness of the  $\text{TiO}_2$  layer was about  $5 \mu\text{m}$ , as shown in the cross-sectional SEM image (Figure 3). Figure 4(a) shows the SEM images of PbS QDs with a higher degree of porosity on the  $\text{TiO}_2$  surface. The deposited PbS QDs and CdS/ZnS layers reduced the porosity between  $\text{TiO}_2$  round-shaped structures, as shown in Figures 4(b) and 4(c), respectively. Lower porosity facilitates charge transfer between PbS QDs and  $\text{TiO}_2$  and causes more energetic injection of electrons produced by PbS QDs into the  $\text{TiO}_2$  conduction band. Energy dispersive X-ray spectroscopy (EDS) revealed the weights of elements present and their atomic percentages. The number of spherical clusters detected on the surface of  $\text{TiO}_2$  electrodes increased as the number of layers increased. Figure 5 indicates that PbS QDs and coating layers were formed on the  $\text{TiO}_2$  surface. Consequently, photovoltaic properties were enhanced when PbS QDs with coating layers were deposited on the  $\text{TiO}_2$  surface [13, 14].

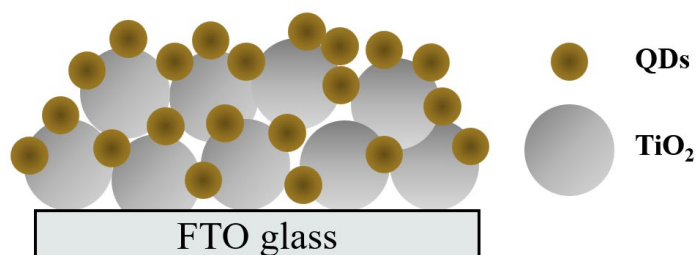


Figure 2. Schematic diagram of deposited QDs on  $\text{TiO}_2$  electrode

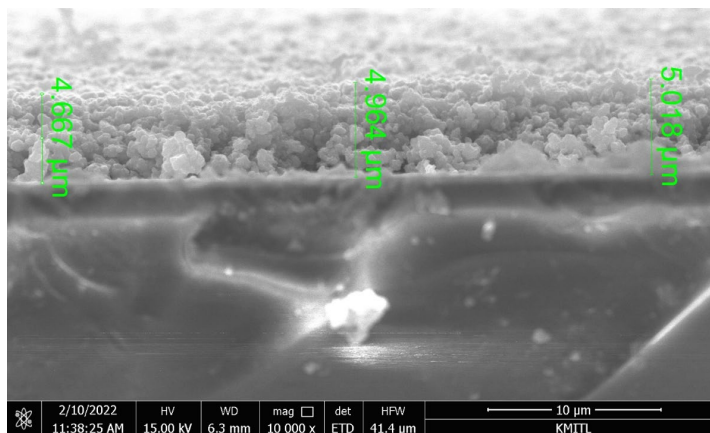
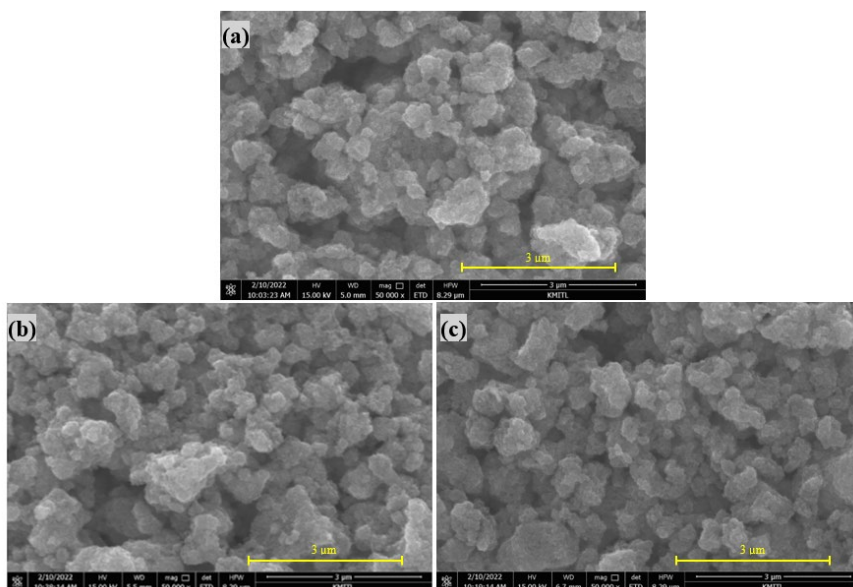
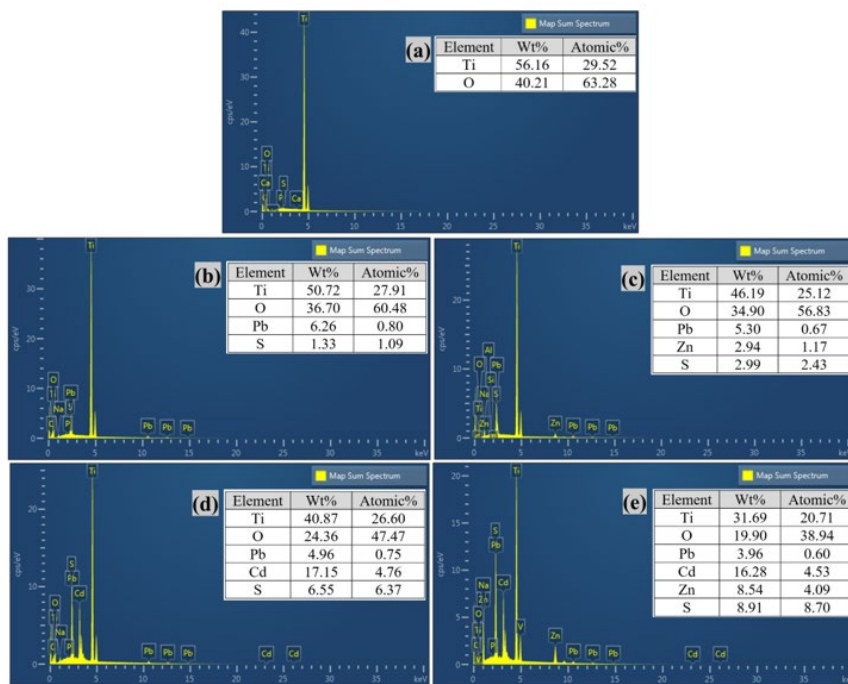


Figure 3. Cross-sectional SEM image of  $\text{TiO}_2$  thin film layer



**Figure 4.** SEM images of: (a)  $\text{TiO}_2$  (b)  $\text{TiO}_2/\text{PbS}$  CQDs (c)  $\text{TiO}_2/\text{PbS}$  CQDs with CdS/ZnS layers



**Figure 5.** Energy dispersive X-ray spectroscopy spectra of: (a)  $\text{TiO}_2$  (b)  $\text{TiO}_2/\text{PbS}$  CQDs (c)  $\text{TiO}_2/\text{PbS}$  CQDs/ZnS (d)  $\text{TiO}_2/\text{PbS}$  CQDs/CdS (e)  $\text{TiO}_2/\text{PbS}$  CQDs/CdS/ZnS

The crystalline structure and phase of nanomaterials with a slightly amorphous background were verified using X-ray diffraction analysis. Figure 6 shows the structural characterization of TiO<sub>2</sub> and PbS CQDs by XRD analysis in the angle 2θ range of 10° to 90°. All diffraction peaks correspond to the tetragonal structure of anatase TiO<sub>2</sub> (JCPDS No. 01-075-1537) and the cubic phase of PbS (JCPDS No. 00-001-0880). The X-ray diffraction patterns show only TiO<sub>2</sub> and PbS planes without crystalline CdS and ZnS planes because their quantities were insufficient [15, 16]. The X-ray diffraction patterns of PbS CQDs consist of diffraction peaks that correspond to planes (200), (220), and (311). Rigaku software and Scherrer's equation (1) were used to calculate the average size of crystallite.

$$D = \frac{0.94\lambda}{\beta \cos\theta} \quad (1)$$

D is the crystallite size, K is a shape factor equal to 0.94, λ is the X-ray wavelength equal to 1.54 angstrom, β is the full width at half maximum (FWHM) in radians, and θ is the half diffraction of angle. According to Rigaku software and equation (1), the average crystallite size of PbS CQDs was around 6.72±0.09 nm.

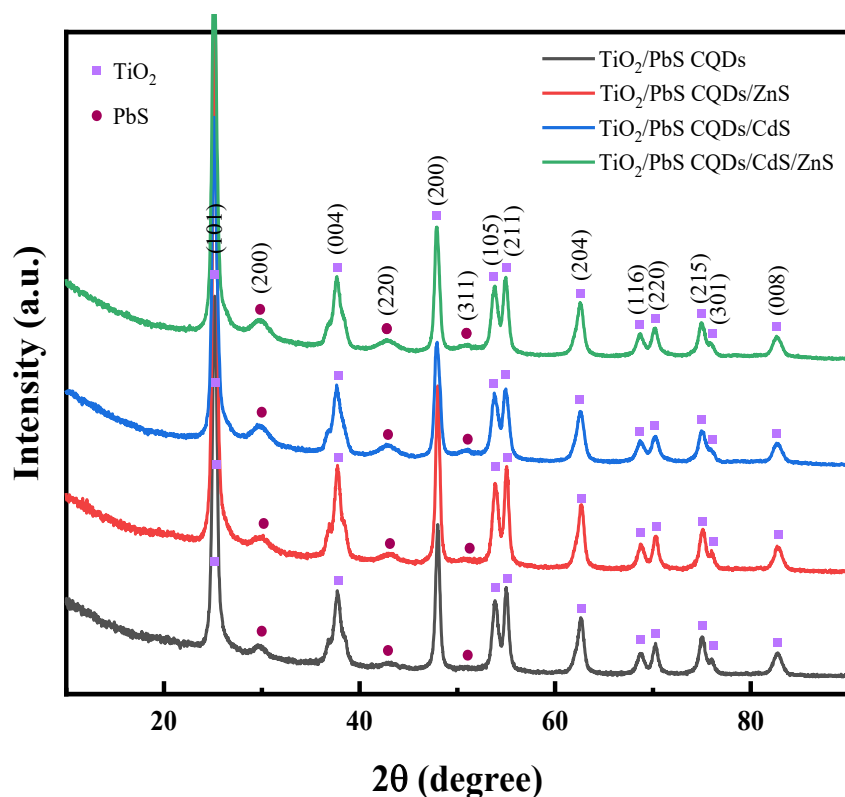


**Figure 6.** XRD patterns of TiO<sub>2</sub>/PbS CQDs with various coating layers

Figures 7-9 show that the optical properties of TiO<sub>2</sub>, ZnS, and CdS electrodes as analyzed using UV-visible spectroscopy and a corresponding Tauc plot. Their absorption edges occurred at about 390, 350, and 500 nm, respectively. PbS CQDs dispersed in chloroform were analyzed using

UV-visible spectroscopy further since the TiO<sub>2</sub>/PbS electrode had low UV-visible absorption. Figure 10 shows the optical band gap of PbS QDs dispersed in chloroform. Their optical band gap and particle size were found to be 1.02 eV and 4.21 nm, respectively, which were consistent with Moreels' study. Nevertheless, the crystallite size calculated with Rigaku software and Scherrer's equation is slightly larger than the particle size dispersed in liquid because of the deposition of PbS QDs on the TiO<sub>2</sub> surface [15]. Table 1 shows the experimental results compared to their literature values.

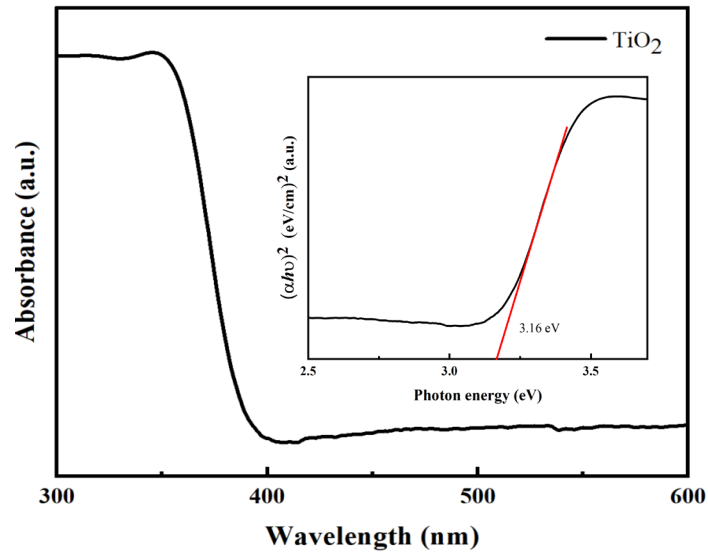


Figure 7. UV-visible absorbance spectra of TiO<sub>2</sub>. Inset: Corresponding Tauc plot

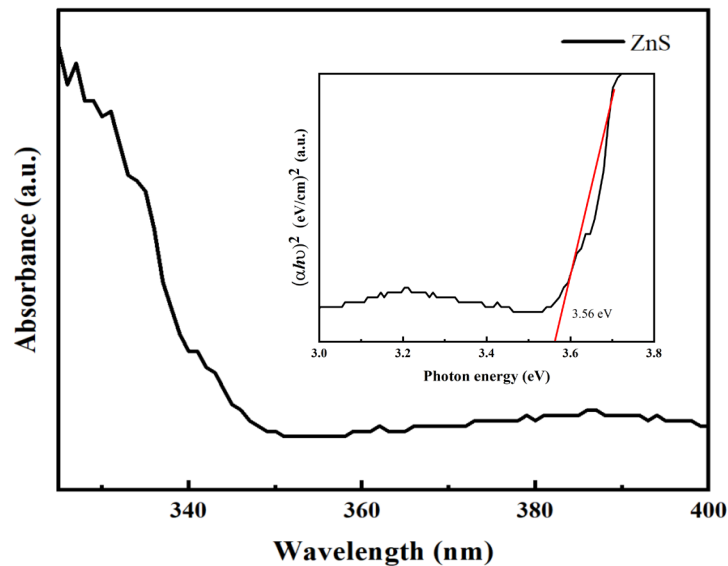


Figure 8. UV-visible absorbance spectra of ZnS. Inset: Corresponding Tauc plot

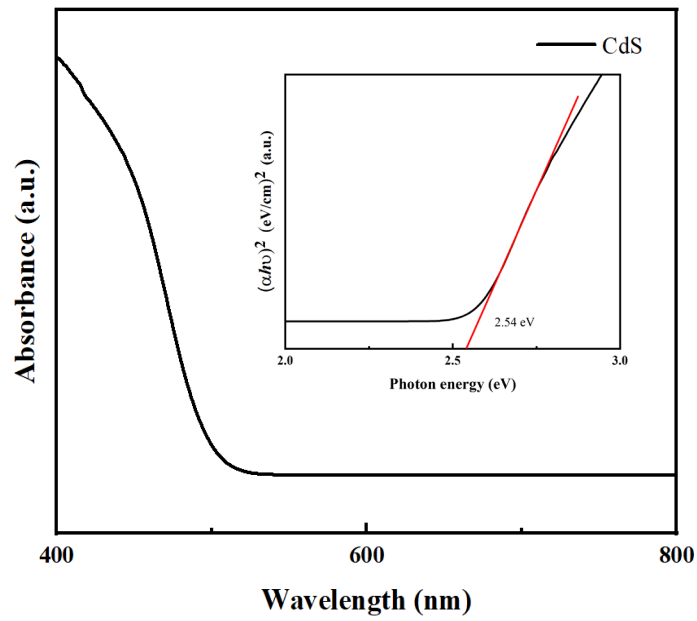


Figure 9. UV-visible absorbance spectra of CdS. Inset: Corresponding Tauc plot

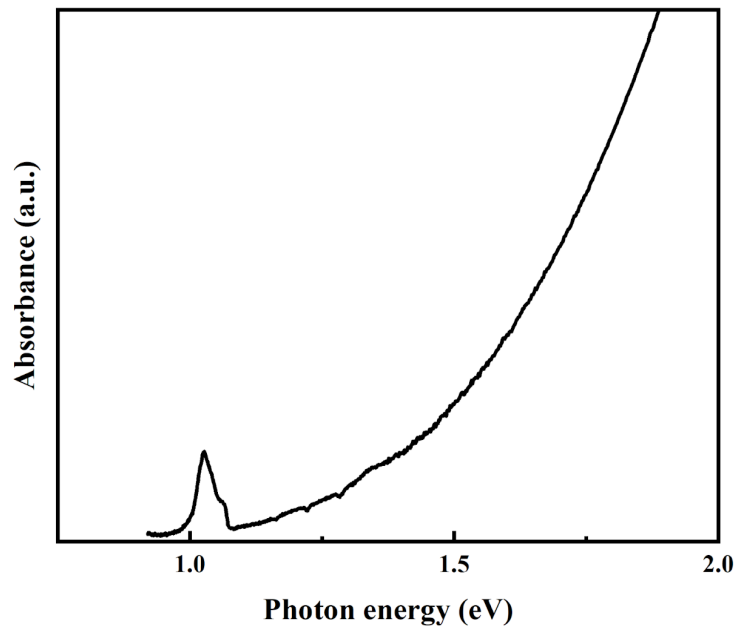


Figure 10. The optical band gap of PbS CQDs dispersed in chloroform

**Table 1.** Optical band gaps of TiO<sub>2</sub>, ZnS, CdS, and PbS CQDs compared to their literature values

Materials	The optical band gap (eV)		References
	Experimental results	literature values	
TiO <sub>2</sub>	3.16	3.20	Dette <i>et al.</i> [17]
ZnS	3.56	3.44-3.56	Lindroos <i>et al.</i> [18]
CdS	2.54	2.42-2.82	Kyobe <i>et al.</i> [19]
PbS	1.02	0.71-1.28	Moreels <i>et al.</i> [20]

Figure 11 shows the absorbance spectra of photoelectrodes, which were characterized by UV-visible spectroscopy. The TiO<sub>2</sub>/PbS CQDs electrode has poor absorption of UV-visible light. The absorption of the other photoelectrodes shifted towards longer wavelengths, and absorbances increased when coating layers were added to the photoelectrodes. The optical properties of lead sulfide appeared low when the TiO<sub>2</sub>/PbS CQDs electrode was analyzed for absorption because the light source was used to generate light in UV-visible spectra. It was reasonable to expect that the TiO<sub>2</sub>/PbS CQDs electrode may have absorbed light at a higher wavelength range [14]. Furthermore, this indicated that adding CdS and ZnS layers enhanced the light-harvesting performance of photoelectrodes more than the TiO<sub>2</sub>/PbS CQDs electrode, which did not have coating layers. Consequently, the assumption was supported by calculating the optical bandgap using equation (2) based on Moreels' study [20].

$$E_g = 0.41 + \frac{1}{0.0252d^2 + 0.283d} \quad (2)$$

where  $E_g$  is the optical band gap, and  $d$  is a particle or crystallite size, employing the size obtained by X-ray diffraction. The optical band gap was found to be 0.72-0.75 eV.

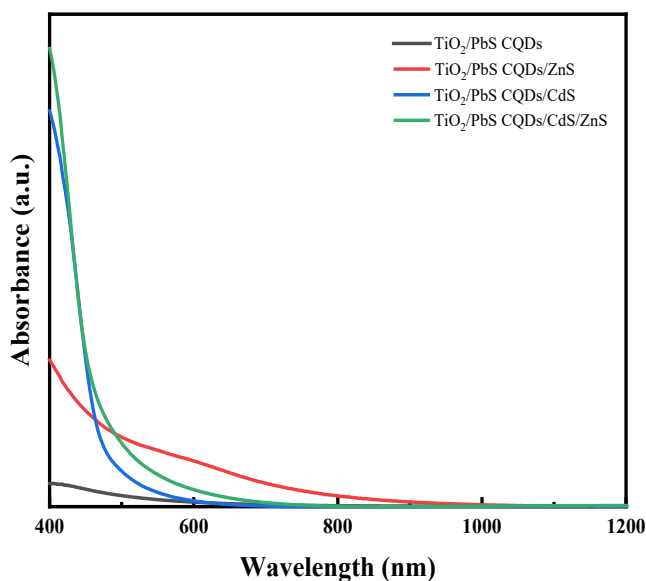
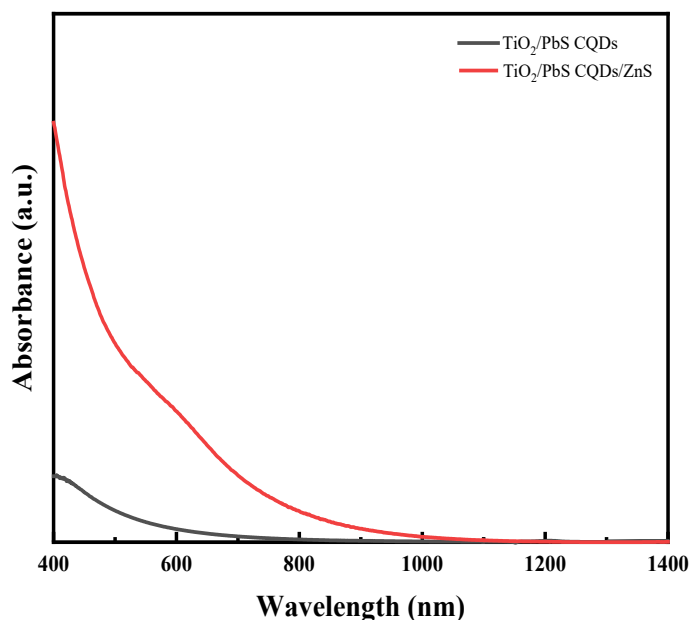
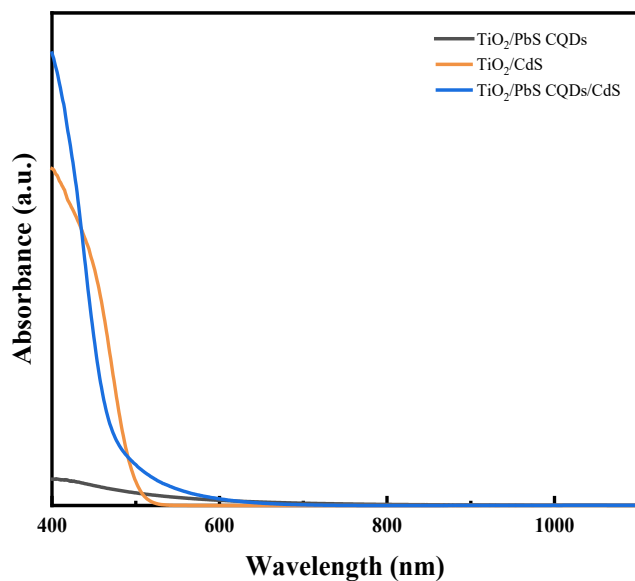
**Figure 11.** The UV-visible absorbance spectra of TiO<sub>2</sub> electrode with PbS CQDs deposits and with various coating layers

Figure 12 shows the UV-visible absorbance spectra of TiO<sub>2</sub>/PbS CQDs and TiO<sub>2</sub>/PbS CQDs/ZnS electrodes for comparison. The TiO<sub>2</sub>/PbS CQDs/ZnS electrode increased absorbance because ZnS was deposited on the TiO<sub>2</sub>/PbS CQDs electrode surface making the surface darker with an increased amount of ZnS [15]. This ZnS layer caused the UV-visible absorbance spectra of the TiO<sub>2</sub>/PbS CQDs electrode to grow. In addition, the UV-visible absorbance spectra of the TiO<sub>2</sub>/PbS CQDs/CdS electrode showed an absorption wavelength at about 650 nm because the absorption edge of the TiO<sub>2</sub>/CdS electrode occurred at around 500 nm. Thus, the maximum wavelength range that TiO<sub>2</sub>/PbS CQDs/CdS electrode could absorb was 400-700 nm. The UV-visible absorbance spectra of TiO<sub>2</sub>/PbS CQDs, TiO<sub>2</sub>/CdS, and TiO<sub>2</sub>/PbS CQDs/CdS electrodes are shown in Figure 13 for comparison. The absorbance spectra of the TiO<sub>2</sub>/PbS CQDs/CdS/ZnS electrode had a shorter wavelength range than the TiO<sub>2</sub>/PbS CQDs/ZnS electrode since ZnS was deposited on CdS layers, and it made the surface darker yellow. Consequently, the UV-visible absorbance spectra of the TiO<sub>2</sub>/PbS CQDs/CdS/ZnS electrode grew in the 400-700 nm range.

The power conversion efficiency was studied using a solar simulation (AM 1.5 G) under illumination conditions (100 mW/cm<sup>2</sup>) at room temperature. The schematic diagram of the working principle of a typical quantum dot solar cell is shown in Figure 14. The electron is excited into the conduction band (CB) of QDs, while the hole stays in the valence band (VB). The electron from the excited CB of QDs is injected into the CB of anatase TiO<sub>2</sub>. The injected electron from QDs percolates through the porous TiO<sub>2</sub> layer and eventually reaches the FTO glass. It then passes through the external load before returning to the Cu<sub>2</sub>S electrode to complete the circuit.



**Figure 12.** UV-visible absorbance spectra of TiO<sub>2</sub>/PbS and TiO<sub>2</sub>/PbS/ZnS electrodes



**Figure 13.** UV-visible absorbance spectra of  $\text{TiO}_2/\text{PbS}$  CQDs,  $\text{TiO}_2/\text{CdS}$ , and  $\text{TiO}_2/\text{PbS}$  CQDs/CdS electrodes

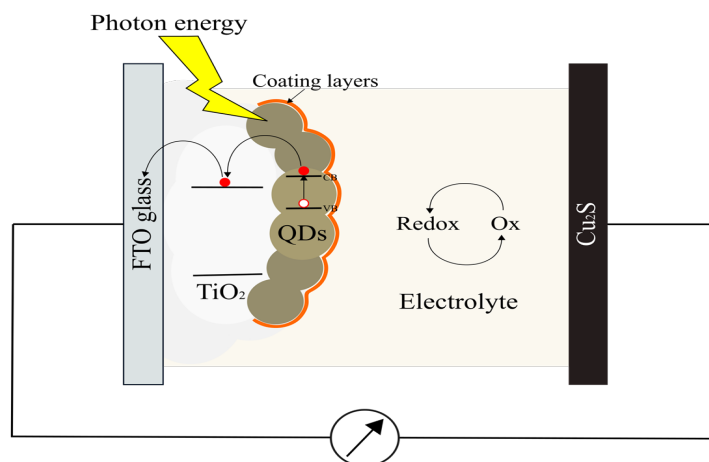


**Figure 14.** Working principle of a typical quantum dot solar cell

The photovoltaic cell parameters of  $\text{TiO}_2$ ,  $\text{TiO}_2/\text{ZnS}$ , and  $\text{TiO}_2/\text{PbS}$  CQDs electrodes were quite unsatisfactory without coating layers. The power conversion efficiency (PCE) of  $\text{TiO}_2$  and  $\text{TiO}_2/\text{ZnS}$  without PbS CQDs electrodes is poor because of the wide optical band gap, which requires more energy to excite an electron to the conduction band and affects the fill factor of photovoltaic cells [21]. Consequently, several metal sulfide ions, such as PbS, CdS,  $\text{Bi}_2\text{S}_3$ , and  $\text{Ag}_2\text{S}$ , can be interesting candidates as sensitizers for wide band gap materials [22]. Table 2 shows the condition of coating layers that influenced photovoltaic cell parameters such as short-circuit current density ( $J_{sc}$ ), open-circuit voltage ( $V_{oc}$ ), fill factor, and PCE.

**Table 2.** The average photovoltaic cell parameters and standard deviations of photoelectrodes under one sun illumination

Condition	$J_{sc}$ [mA/cm <sup>2</sup> ]	$V_{oc}$ [volt]	Fill factor	PCE [%]
TiO <sub>2</sub>	0.90±0.34	0.19±0.03	0.21±0.01	0.05±0.01
TiO <sub>2</sub> /ZnS	1.13±0.33	0.37±0.02	0.18±0.06	0.06±0.01
TiO <sub>2</sub> /PbS CQDs	1.16±0.16	0.36±0.01	0.56±0.05	0.22±0.01
TiO <sub>2</sub> /CdS	2.59±0.03	0.41±0.03	0.48±0.09	0.57±0.11
TiO <sub>2</sub> /PbS CQDs/ZnS	2.82±0.04	0.43±0.01	0.49±0.02	0.59±0.05
TiO <sub>2</sub> /PbS CQDs/CdS	3.21±0.09	0.44±0.01	0.56±0.01	0.78±0.02
TiO <sub>2</sub> /PbS CQDs/CdS/ZnS	3.41±0.03	0.52±0.01	0.58±0.01	1.01±0.02

The efficiency of TiO<sub>2</sub>/PbS CQDs electrodes tended to rise when the coating layers were modified. Electrons from PbS efficiently react with the polysulfide electrolyte when light is absorbed due to the narrow band gap (0.41-1.28 eV) [22]. Thus, the TiO<sub>2</sub>/PbS CQDs electrode needed to be passivated by CdS and ZnS coating layers. The short-circuit current density ( $J_{sc}$ ) and open-circuit voltage ( $V_{oc}$ ) were significantly raised from 1.16 mA/cm<sup>2</sup> to 3.41 mA/cm<sup>2</sup> and 0.36 V to 0.52 V, respectively, as the various coating layers were applied. The increased current density of TiO<sub>2</sub>/PbS CQDs, TiO<sub>2</sub>/PbS CQDs/ZnS, TiO<sub>2</sub>/PbS CQDs/CdS, and TiO<sub>2</sub>/PbS CQDs/CdS/ZnS corresponded with the optical properties analyzed by UV-visible spectroscopy.

Furthermore, it was demonstrated that cadmium sulfide and zinc sulfide coating layers were applied to increase photocurrent and power conversion efficiency due to the rising absorption light [23].

#### 4. Conclusions

We reported on an elementary method for synthesizing PbS CQDs by the co-precipitation method on the TiO<sub>2</sub> electrode. PbS CQDs diffraction peaks corresponded to the cubic phase with a crystallite size of around 6-7 nm. The calculated optical band gap of photoelectrodes was found to be 0.72-0.75 eV when the crystallite size was substituted into the equation based on Moreels' study. Furthermore, PbS CQDs dispersed in chloroform were analyzed. Their optical band gap and particle size were around 1.02-1.03 eV and 4-5 nm, respectively. Under one sun illumination, the TiO<sub>2</sub>/PbS CQDs electrode with CdS and ZnS layers obtained the highest current density of 3.41 mA/cm<sup>2</sup> and the maximum power conversion efficiency of 1.01%. The improved photovoltaic cell performance was related to the extended light-harvesting quantity of the TiO<sub>2</sub>/PbS CQDs electrode. CdS and ZnS layers improved power conversion efficiency compared to TiO<sub>2</sub>/PbS CQDs electrodes.

These studies offer evidence that CdS and ZnS layers effectively improve photovoltaic cell absorbance and electrical properties. We conclude that these initial results indicate that the CdS and ZnS layers can enhance light absorption and photovoltaic properties. Further studies are needed to establish whether these findings can be applied to perovskite solar cells [24-26].

#### 5. Acknowledgements

This research was supported by Faculty of Science, King Mongkut's Institute of Technology Ladkrabang.

## References

- [1] Rosiles-Perez, C., Serrano-Estrada, M.A., Sidhik, S., Alatorre-Ordaz, A., Torres-Castro, A., Vallejo, M.A., Jiménez-González, A.E. and López-Luke, T., 2020. Synthesis of high quality PbS colloidal quantum dots by ultrasonic bath as photosensitizers in a TiO<sub>2</sub> solar cell. *Journal of Solid State Chemistry*, 292, DOI: 10.1016/j.jssc.2020.121720.
- [2] Rühle, S., Shalom, M. and Zaban, A., 2010. Quantum-dot-sensitized solar cells. *Chem Phys Chem*, 11(11), 2290-2304, DOI: 10.1002/cphc.201000069.
- [3] Sadovnikov, S.I., Gusev, A.I. and Rempel, A.A., 2016. Nanostructured lead sulfide: synthesis, structure and properties. *Russian Chemical Reviews*, 85(7), 731-758, DOI: 10.1070/RCR4594.
- [4] Chistyakov, A.A., Zvaigzne, M.A., Nikitenko, V.R., Tameev, A.R., Martynov, I.L. and Prezhdo, O.V., 2017. Optoelectronic properties of semiconductor quantum dot solids for photovoltaic applications. *Journal of Physical Chemistry Letters*, 8(17), 4129-4139, DOI: 10.1021/acs.jpcclett.7b00671.
- [5] Beygi, H., Sajjadi, S.A., Babakhani, A., Young, J.F. and van Veggel, F.C.J.M., 2018. Surface chemistry of as-synthesized and air-oxidized PbS quantum dots. *Applied Surface Science*, 457, 1-10, DOI: 10.1016/j.apsusc.2018.06.152.
- [6] Jiao, S., Wang, J., Shen, Q., Li, Y. and Zhong, X., 2016. Surface engineering of PbS quantum dot sensitized solar cells with a conversion efficiency exceeding 7%. *Journal of Materials Chemistry A*, 4(19), 7214-7221, DOI: 10.1039/c6ta02465c.
- [7] Chang, J. and Waclawik, E.R., 2014. Colloidal semiconductor nanocrystals: Controlled synthesis and surface chemistry in organic media. *RSC Advances*, 4(45), 23505-23527, DOI: 10.1039/c4ra02684e.
- [8] Zhou, Y., Zhao, H., Ma, D. and Rosei, F., 2018. Harnessing the properties of colloidal quantum dots in luminescent solar concentrators. *Chemical Society Reviews*, 47(15), 5866-5890, DOI: 10.1039/c7cs00701a.
- [9] Zheng, S., Chen, J., Johansson, E.M.J. and Zhang, X., 2020. PbS Colloidal quantum dot inks for infrared solar cells. *iScience*, 23(11), DOI: 10.1016/j.isci.2020.101753.
- [10] Schüth, F. and Unger, K., 1999. Precipitation and coprecipitation. In: G. Ertl, H. Knözinger and J. Weitkamp, eds. *Preparation of Solid Catalysts*. Munich: Wiley Online Library, pp. 60-84.
- [11] Hachiya, S., Shen, Q. and Toyoda, T., 2012. Effect of ZnS coatings on the enhancement of the photovoltaic properties of PbS quantum dot-sensitized solar cells. *Journal of Applied Physics*, 111(10), DOI: 10.1063/1.4720468.
- [12] Tavakoli, M.M., 2016. Surface Engineering of Pbs colloidal quantum dots using atomic passivation for photovoltaic applications. *Procedia Engineering*, 139(21), 117-122, DOI: 10.1016/j.proeng.2015.08.1122.
- [13] Im, S.H., Kim, H.J., Kim, S.W., Kim, S.W. and Seok, S.I., 2011. All solid state multiply layered PbS colloidal quantum-dot-sensitized photovoltaic cells. *Energy and Environmental Science*, 4(10), 4181-4186, DOI: 10.1039/c1ee01774h.
- [14] Kim, H.J., Lee, H.D., Kumar, C.S.S.P., Rao, S.S., Chung, S.H. and Punnoose, D., 2015. The effect of manganese in a CdS/PbS colloidal quantum dot sensitized TiO<sub>2</sub> solar cell to enhance its efficiency. *New Journal of Chemistry*, 39(6), 4805-4813, DOI: 10.1039/c5nj00400d.
- [15] Sun, L., Koh, Z.Y. and Wang, Q., 2013. PbS quantum dots embedded in a ZnS dielectric matrix for bulk heterojunction solar cell applications. *Advanced Materials*, 25(33), 4598-4604, DOI: 10.1002/adma.201301544.
- [16] Jostar, T.S., Devadason, S. and Suthagar, J., 2015. Influence of Mn-doping with CdS on the structural and optical properties of ZnS/CdS/TiO<sub>2</sub> photoanodes. *Journal of Materials Science: Materials in Electronics*, 26(8), 5668-5676, DOI: 10.1007/s10854-015-3117-x.

- 
- [17] Dette, C., Pérez-Osorio, M.A., Kley, C.S., Punke, P., Patrick, C.E., Jacobson, P., Giustino, F., Jung, S.J. and Kern, K., 2014. TiO<sub>2</sub> anatase with a bandgap in the visible region. *Nano Letters*, 14(11), 6533-6538, DOI: 10.1021/nl503131s.
- [18] Lindroos, S., Kanninen, T. and Leskelä, M., 1997. Growth of zinc sulfide thin films by the successive ionic layer adsorption and reaction (SILAR) method on polyester substrates. *Materials Research Bulletin*, 32(12), 1631-1636, DOI: 10.1016/S0025-5408(97)00155-4.
- [19] Kyobe, J.W., Mubofu, E.B., Makame, Y.M.M., Mlowe, S. and Revaprasadu, N., 2016. Cadmium sulfide quantum dots stabilized by castor oil and ricinoleic acid. *Physica E: Low-Dimensional Systems and Nanostructures*, 76, 95-102, DOI: 10.1016/j.physe.2015.10.008.
- [20] Moreels, I., Lambert, K., Smeets, D., De Muynck, D., Nollet, T., Martins, J.C., Vanhaecke, F., Vantomme, A., Delerue, C., Allan, G. and Hens, Z., 2009. Size-dependent optical properties of colloidal PbS quantum dots. *ACS Nano*, 3(10), 3023-3030, DOI: 10.1021/nn900863a.
- [21] Anitha, B., Vijith, K.P., Alexander, A., Srivastava, V. and Namboothiry, M.A.G., 2020. Understanding the poor fill factor of solution-processed squaraine based solar cells in terms of charge carrier dynamics probed via impedance and transient spectroscopy. *Journal of Materials Chemistry C*, 8(42), 14748-14756, DOI: 10.1039/d0tc03012k.
- [22] Yang, S.M., Huang, C.H., Zhai, J., Wang, Z.S. and Jiang, L., 2002. High photostability and quantum yield of nanoporous TiO<sub>2</sub> thin film electrodes co-sensitized with capped sulfides. *Journal of Materials Chemistry*, 12(5), 1459-1464, DOI: 10.1039/b105796k.
- [23] Sato, K., Ono, K., Izuishi, T., Kuwahara, S., Katayama, K., Toyoda, T., Hayase, S. and Shen, Q., 2016. The effect of CdS on the charge separation and recombination dynamics in PbS/CdS double-layered quantum dot sensitized solar cells. *Chemical Physics*, 478, 159-163, DOI: 10.1016/j.chemphys.2016.03.014.
- [24] Yang, Z., Janmohamed, A., Lan, X., García De Arquer, F.P., Voznyy, O., Yassitepe, E., Kim, G.H., Ning, Z., Gong, X., Comin, R. and Sargent, E.H., 2015. Colloidal quantum dot photovoltaics enhanced by Perovskite shelling. *Nano Letters*, 15(11), 7539-7543, DOI: 10.1021/acs.nanolett.5b03271.
- [25] Andruszkiewicz, A., Zhang, X., Johansson, M.B., Yuan, L. and Johansson, E.M.J., 2021. Perovskite and quantum dot tandem solar cells with interlayer modification for improved optical semitransparency and stability. *Nanoscale*, 13(12), 6234-6240, DOI: 10.1039/d0nr08375e.
- [26] Chen, H., Pina, J.M., Hou, Y. and Sargent, E.H., 2021. Synthesis, applications, and prospects of quantum-dot-in-Perovskite solids. *Advanced Energy Materials*, 12(4), DOI: 10.1002/aenm.202100774.